J|A|C|S
ARTICLES
Published on Web 05/10/2006

Stepwise Formation and Characterization of Covalently Linked Multiporphyrin−Imide Architectures on Si(100)

Jieying Jiao,[†] Franklin Anariba,[†] Hugo Tiznado,[†] Izabela Schmidt,[‡] Jonathan S. Lindsey,*[,‡] Francisco Zaera,*[,†] and David F. Bocian*[,†]

Contribution from the Department of Chemistry, University of California, Riverside, California 92521-0403, and Department of Chemistry, North Carolina State University, Raleigh, North Carolina 27695-8204

Received February 7, 2006; E-mail: jlindsey@ncsu.edu, David.Bocian@ucr.edu, Francisco.Zaera@ucr.edu

Abstract: A major challenge in molecular electronics and related fields entails the fabrication of elaborate molecular architectures on electroactive surfaces to yield hybrid molecular/semiconductor systems. A method has been developed for the stepwise synthesis of oligomers of porphyrins linked covalently via imide units. A triallyl−porphyrin bearing an amino group serves as the base unit on Si(100), and the alternating use of a dianhydride (3,3′,4,4′-biphenyltetracarboxylic dianhydride) and a porphyrin−diamine for reaction enables the rapid and simple buildup of oligomers composed of 2−5 porphyrins. The properties of these porphyrin "multad" films on Si(100) were interrogated using a variety of techniques. The charge densities of the redox-active porphyrin oligomers were determined via electrochemical methods. The stepwise growth was evaluated in detail via Fourier transform infrared (FTIR) spectroscopy and by selected X-ray photoelectron spectroscopic (XPS) studies. The morphology was probed via AFM methods. Finally, the thickness was evaluated by using a combination of ellipsometry and AFM height profiling, accompanied by selected XPS studies. Collectively, these studies demonstrate that high charge density, ultrathin, multiporphyrin films of relatively well-controlled thickness can be grown in a stepwise fashion using the imide-forming reaction. The increased charge densities afforded by the porphyrin multads may prove important for the fabrication of molecular-based information-storage devices. This bottom-up process for construction of surface-tethered molecular architectures complements the top-down lithographic approach for construction of functional devices with nanoscale dimensions.

I. Introduction

Over the past six years, we have been developing molecular-based information-storage systems wherein redox-active molecules are employed to store information in the form of electrical charge. This approach is amenable to implementation in a hybrid technology, where the charge-storage molecules replace the material that presently serves as the charge-storage medium in existing memory chips.[1] As part of this program, we have prepared a wide variety of redox-active molecular architectures, particularly porphyrinic molecules, as candidates for information-storage applications.[2−10] The basic design of the information-storage molecules includes the redox-active unit and a tether that terminates in a functional group that can undergo facile covalent attachment to a surface.

A key advantage of employing molecules for charge storage is that molecules afford significantly higher charge density than the materials commonly in use in memory devices. The charge densities achievable with a monolayer of a porphyrin-based storage medium typically fall in the range of 10−40 μC cm^{-2}, depending on the tether and surface-attachment group,[2−12] compared with 1−2 μC cm^{-2} for the Si/SiO$_2$ capacitors currently used in dynamic random access memories.[13] The relatively low

[†] University of California.
[‡] North Carolina State University.

(1) (a) Roth, K. M.; Dontha, N.; Dabke, R. B.; Gryko, D. T.; Clausen, C.; Lindsey, J. S.; Bocian, D. F.; Kuhr, W. G. *J. Vac. Sci. Technol., B.* **2000**, *18*, 2359−2364. (b) Liu, Z.; Yasseri, A. A.; Lindsey, J. S.; Bocian, D. F. *Science* **2003**, *302*, 1543−1545.
(2) Balakumar, A.; Lysenko, A. B.; Carcel, C.; Malinovskii, V. L.; Gryko, D. T.; Schweikart, K.-H.; Loewe, R. S.; Yasseri, A. A.; Liu, Z.; Bocian, D. F.; Lindsey, J. S. *J. Org. Chem.* **2004**, *69*, 1435−1443.
(3) Muthukumaran, K.; Loewe, R. S.; Ambroise, A.; Tamaru, S.-I.; Li, Q.; Mathur, G.; Bocian, D. F.; Misra, V.; Lindsey, J. S. *J. Org. Chem.* **2004**, *69*, 1444−1452.
(4) Loewe, R. S.; Ambroise, A.; Muthukumaran, K.; Padmaja, K.; Lysenko, A. B.; Mathur, G.; Li, Q.; Bocian, D. F.; Misra, V.; Lindsey, J. S. *J. Org. Chem.* **2004**, *69*, 1453−1460.
(5) Wei, L.; Padmaja, K.; Youngblood, W. J.; Lysenko, A. B.; Lindsey, J. S.; Bocian, D. F. *J. Org. Chem.* **2004**, *69*, 1461−1469.
(6) Liu, Z.; Yasseri, A. A.; Loewe, R. S.; Lysenko, A. B.; Malinovskii, V. L.; Zhao, Q.; Surthi, S.; Li, Q.; Misra, V.; Lindsey, J. S.; Bocian, D. F. *J. Org. Chem.* **2004**, *69*, 5568−5577.
(7) Lysenko, A. B.; Malinovskii, V. L.; Kisari, P.; Wei, L.; Diers, J. R.; Bocian, D. F.; Lindsey, J. S. *J. Porphyrins Phthalocyanines* **2005**, *9*, 491−508.
(8) Padmaja, K.; Wei, L.; Lindsey, J. S.; Bocian, D. F. *J. Org. Chem.* **2005**, *70*, 7972−7278.
(9) Thamyongkit, P.; Yu, L.; Padmaja, K.; Jiao, J.; Bocian, D. F.; Lindsey, J. S. *J. Org. Chem.* **2006**, *71*, 1156−1171.
(10) Schmidt, I.; Jiao, J.; Thamyongkit, P.; Sharada, D. S.; Bocian, D. F.; Lindsey, J. S. *J. Org. Chem.* **2006**, *71*, 3033−3050.
(11) Roth, K. M.; Yasseri, A. A.; Liu, Z.; Dabke, R. B.; Malinovskii, V.; Schweikart, K.-H.; Yu, L.; Tiznado, H.; Zaera, F.; Lindsey, J. S.; Kuhr, W. G.; Bocian, D. F. *J. Am. Chem. Soc.* **2003**, *125*, 505−517.
(12) Liu, Z.; Schmidt, I.; Thamyongkit, P.; Loewe, R. S.; Sykomin, D.; Diers, J. R.; Zhao, Q.; Misra, V.; Lindsey, J. S.; Bocian, D. F. *Chem. Mater.* **2005**, *17*, 3728−3742.
(13) (a) Mandelman, J. A.; Dennard, R. H.; Bronner, G. B.; DeBrosse, J. K.; Divakaruni, R.; Li, Y.; Radens, C. J. *IBM J. Res. Dev.* **2002**, *46*, 187−212. (b) Kuhr, W. G.; Gallo, A. R.; Manning, R. W.; Rhodine, C. W. *Mater. Res. Soc. Bull.* **2004**, 838−842.

charge densities afforded by the latter capacitors necessitates the use of stack or trench architectures with very high aspect ratios to store sufficient charge for reliable readout. The fabrication of such nanoscale structures with high aspect ratios requires elaborate lithographic manufacturing procedures.[13] The much higher charge densities afforded by the porphyrin-based storage medium would permit the use of more planar architectures, significantly simplifying the manufacturing process. Despite the fact that porphyrin monolayers afford superior charge densities at the current feature sizes of devices, still higher charge densities will be desirable as the feature sizes become smaller. Toward this goal, we have investigated a variety of dyadic and polymeric porphyrin architectures that utilize the vertical dimension to increase the effective surface coverage of the porphyrins and, hence, increase the charge density.[9,12] Extremely high charge densities can be achieved with polymeric porphyrin films; however, the polymer-forming reaction does not afford particularly good control of the film thickness, particularly when relatively thin films (3−10 porphyrins) are desired.[12]

Recently, we have developed a strategy for stepwise growth of a polyimide construct on top of a base porphyrin monolayer attached to a Si(100) substrate.[10] The base monolayer was formed using a porphyrin that is functionalized with a triallyl group for surface attachment and an opposing *p*-aminophenyl group for imide formation (porphyrin **1**, Chart 1). The monolayer was then reacted in successive steps, first with a dianhydride (BPTC, Chart 1) and then with a dianiline derivative (MDA, Chart 1). This process was repeated to obtain a polyimide covalently linked to the porphyrin base layer. This process differs from existing methods for preparing multicomponent molecular architectures, such as the surface-supported synthesis of biomolecules (peptides, nucleic acids), in affording stepwise synthesis of covalently linked architectures without the use of any protecting groups. The method is also distinct from methods used to prepare multilayer assemblies or thin films, such as Langmuir−Blodgett techniques or zirconium−phosphate linking chemistry.[14] In some sense, our methodology is similar to an atomic layer deposition (ALD) process[15] wherein two self-limiting and complementary reactions afford controlled stepwise synthesis on a surface. We note that Blanchard has reported the stepwise growth of covalently linked polymer multilayers on a surface wherein a layer of laterally deposited polymer is attached to the lower layer via a monomeric interconnect having complementary functional groups; successive buildup affords covalently interconnected, laterally organized polymer multilayers.[16] By contrast, the method we employ affords a general approach for the controlled formation of ultrathin films composed of surface-attached oligomers without explicit lateral cross-links.

A key attraction of the polyimide constructs, in addition to amenability to stepwise fabrication with control over the composition of each monomeric unit, lies in the high thermal stability (∼400 °C) and redox stability of the corresponding imide polymers.[17] Stability at high temperature is essential for use in semiconductor fabrication processes, and redox stability is essential for use in an electrically addressable memory cell. In our initial studies, the porphyrin formed the base layer whereas all successive components were composed of (non-porphyrin) arylimide constituents. The success of the imide-forming process prompted us to explore the stepwise formation of multiporphyrin architectures wherein MDA is replaced with a bis(aminophenyl)-functionalized porphyrin (porphyrins **2** and **3**, Chart 1).

Herein, we report on the preparation and characterization of

Chart 1

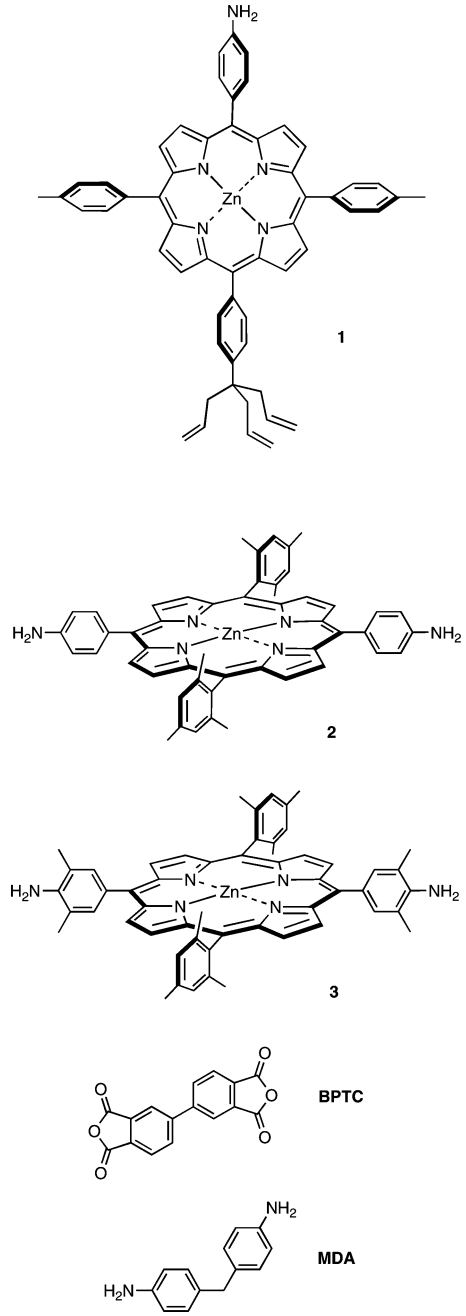

(14) (a) Vioux, A.; Le Bideau, J.; Mutin, P. H.; Leclercq, D. *Top. Curr. Chem.* **2004**, *232*, 145−174. (b) *Multilayer Thin Films*; Decher, G., Schlenoff, J. B., Eds.; Wiley-VCH: Weinheim, 2002. (c) Manne, S.; Aksay, I. A. *Curr. Opin. Solid State Mater. Sci.* **1997**, *2*, 358−364. (d) Tredgold, R. H. *Order in Thin Organic Films*; Cambridge University Press: Cambridge, UK, 1994. (e) Cao, G.; Hong, H.-G.; Mallouk, T. E. *Acc. Chem. Res.* **1992**, *25*, 420−427. (f) Ulman, A. *An Introduction to Ultrathin Organic Films*; Academic Press: Boston, 1991.

(15) (a) Leskelä, M.; Ritala, M. *Angew. Chem., Int. Ed.* **2003**, *42*, 5548−5554. (b) Lim, B. S.; Rahtu, A.; Gordon, R. G. *Nat. Mater.* **2003**, *2*, 749−754.

(16) (a) Major, J. S.; Blanchard, G. J. *Chem. Mater.* **2002**, *14*, 2574−2581. (b) Kohli, P.; Blanchard, G. J. *Langmuir* **2000**, *16*, 8518−8524.

(17) (a) Xie, W.; Pan, W.-P.; Chuang, K. C. *Thermochim. Acta* **2001**, *367*−368, 143−153. (b) Cella, J. A. *Polym. Degrad. Stab.* **1992**, *36*, 99−110.

Chart 2

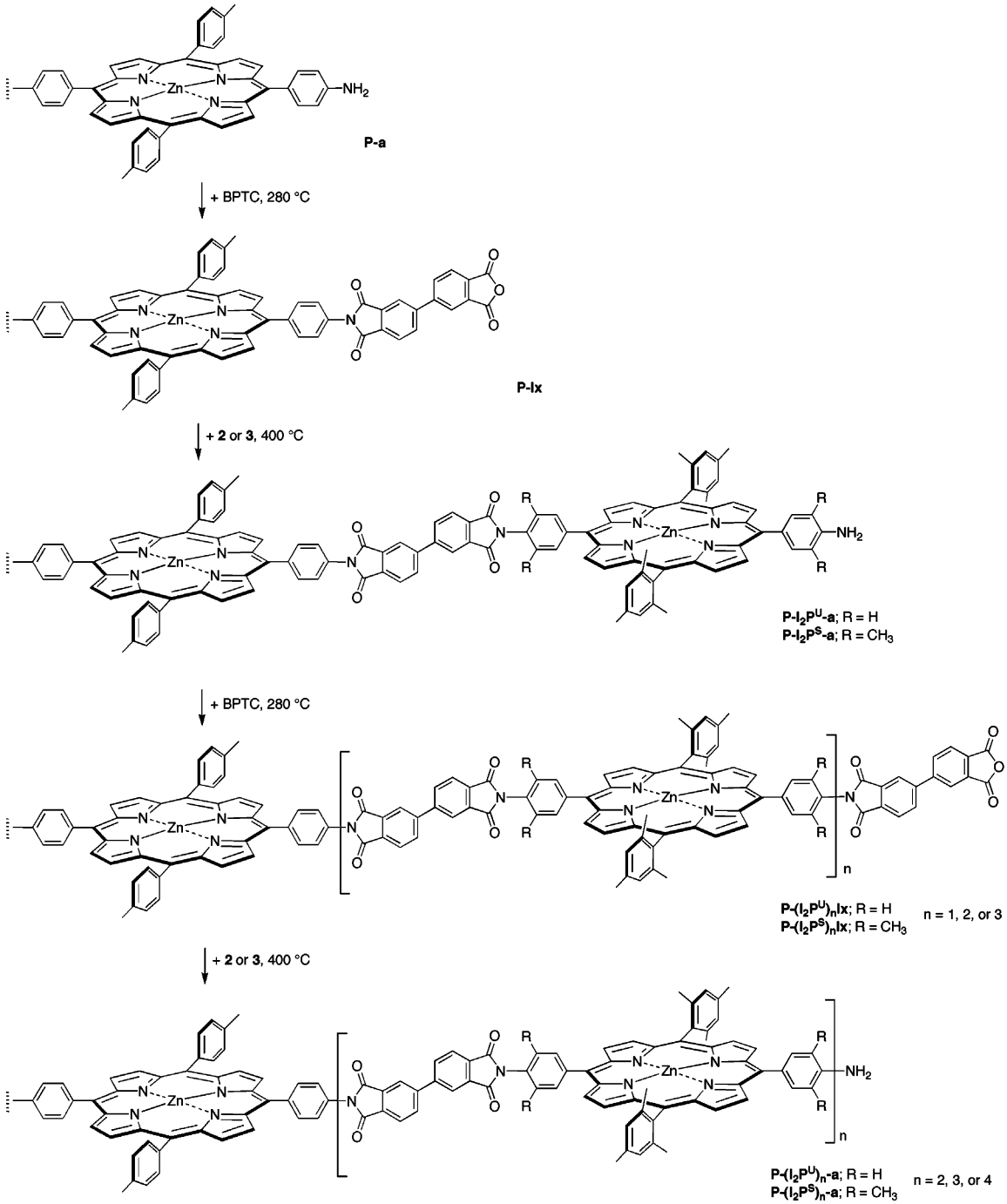

multiporphyrin architectures (multads) composed of 2−5 porphyrins. The anhydride-terminated intermediates were also investigated. The structures of the various oligomers are shown in Chart 2. The properties of the porphyrin multad films on Si(100) were interrogated using a variety of techniques as follows: (1) The charge densities were determined via electrochemical methods. (2) The stepwise growth was evaluated in detail via Fourier transform infrared (FTIR) spectroscopy and by selected X-ray photoelectron spectroscopic (XPS) studies. (3) The morphology was probed via AFM methods. (4) The thickness was evaluated by using a combination of ellipsometry and AFM height profiling, again accompanied by selected XPS studies. Collectively, these studies demonstrate that ultrathin, multiporphyrin films of relatively well-controlled thickness can be grown in a stepwise fashion using the imide-forming reaction. This in turn affords control over the achievable charge density on the substrate, which may prove important for the fabrication of molecular-based information-storage devices. This bottom-up process for construction of surface-tethered molecular architectures complements the top-down lithographic approach for construction of functional devices with nanoscale dimensions.

II. Experimental Section

A. General. All porphyrins were synthesized as described previously.[10] The substrates for surface attachment were prepared from commercially available highly doped *p*-type Si(100) wafers. The anhydrous solvents and chemicals used in the preparation of the

porphyrin monolayers and the stepwise assembly of the porphyrin multads include benzonitrile, CH_2Cl_2, *N*,*N*-dimethylacetamide (DMAc), and 3,3′,4,4′-biphenyltetracarboxylic dianhydride (BPTC); all were used as received. The propylene carbonate used for the electrochemical studies was dried on molecular sieves before use. The Bu_4NPF_6 supporting electrolyte was recrystallized three times from methanol and dried at 110 °C under vacuum.

B. Porphyrin Monolayer Preparation. The monolayer of **1** on Si(100), designated **P**−**a**, was prepared using a high-temperature (400 °C), short-time (2 min) "baking" attachment procedure described previously.[6] The monolayers for the electrochemical experiments were prepared by dispensing a 2 μL drop of the porphyrin solution onto the surface of a microelectrode contained in a sparged VOC vial sealed under Ar. The monolayers prepared for the FTIR, XPS, ellipsometry, and AFM experiments utilized much larger platforms (∼1 cm^2) and, consequently, required a larger drop size, ∼50 μL. After deposition, the vial containing the Si substrate was heated on a hotplate at 400 °C for 2 min and then removed and purged with Ar while being allowed to cool to room temperature. Finally, the Si substrate was rinsed, sonicated five times with anhydrous CH_2Cl_2, and purged dry with Ar.

C. Porphyrin Multad Preparation. The first step in the studies of stepwise formation of the porphyrin multads was preparation of the **P**−**a** base layer as described above. The cleaned and washed substrate was then placed in a sealed vial and purged with Ar, after which a drop of the solution of BPTC (5 mM in DMAc) was introduced (5 and 50 μL for the electrochemical and other spectroscopic studies, respectively). After deposition, the vial containing the Si substrate was heated on a hotplate at 280 °C for 2 min and then removed and purged with Ar while being allowed to cool to room temperature. Finally, the Si substrate was rinsed, sonicated five times with anhydrous CH_2Cl_2, and purged dry with Ar. The sample was then interrogated using electrochemical or spectroscopic techniques.

In the case of the samples used for the electrochemical or FTIR studies, the successive components were added to the original sample as follows. After electrochemical or FTIR interrogation, the sample was washed and dried, and a solution of **2** or **3** (2 mM in PhCN) was introduced onto the substrate. The sample was then heated at 400 °C for 2 min, removed and purged under Ar until cooled to room temperature, washed and sonicated with CH_2Cl_2, and dried with Ar. It should be noted that a lower temperature (280 °C) was initially used in attempts to form the imide linkage to the porphyrins; however, no reaction appeared to occur, as evidenced by electrochemical and FTIR studies. After the second electrochemical or FTIR interrogation, the sample was rewashed and dried and the above procedure was repeated with alternating doses of BPTC and **2** or **3**.

In the case of the XPS, ellipsometric, and AFM measurements, it proved to be too cumbersome to add components to the original sample and interrogate after each successive step. For these measurements, separate samples of a given composition were individually prepared and interrogated. We assessed this method to be reliable based on electrochemical and FTIR studies, showing that multads formed by successive steps and interrogated at the end of the formation process appeared identical to multads of the same composition that were formed and interrogated in successive steps.

D. Electrochemical Measurements. The electrochemical measurements were performed in a two-electrode configuration using highly doped *p*-type Si(100) working electrodes (100 × 100 μm^2) and a Ag counter/reference electrode, fabricated as described earlier.[11] Propylene carbonate containing 1.0 M *n*-Bu_4NPF_6 was used as solvent/electrolyte. The cyclic voltammograms were recorded using a Gamry Instruments PC4−FAS1 femtostat running PHE 200 framework and Echem Analyst software. The charge density in the film was determined by integration of the total charge of both anodic waves normalized by the geometrical area of the microelectrode. The effective surface coverage of the porphyrins in the multads (measured as moles of porphyrins per cm^2 of surface area) was determined from the charge density, normalized by a factor of 2 to account for the fact that each porphyrin can undergo two oxidations.

E. FTIR Spectroscopy. The FTIR spectra were collected at room temperature with a spectral resolution of 4 cm^{-1} using a Bruker Tensor 27 spectrometer. The IR spectra of the monolayers were obtained using a Harrick Scientific horizontal reflection Ge attenuated total reflection accessory (GATR, 65° incidence angle). The Si substrates were placed in contact with the flat surface of a semispherical Ge crystal that serves as the optical element, and IR spectra were collected with *p*-polarized light using a liquid nitrogen-cooled, medium-bandwidth MCT detector (600−4000 cm^{-1}) and averaging 256 scans. The Ge crystal was cleaned with neat 2-butanone before every experiment, and the GATR accessory was purged with dry N_2 during data acquisition. The spectra of porphyrins were referenced against that of a hydrogen-terminated Si(100) surface previously subjected to the same deposition conditions as those used to obtain the monolayer but using only the neat deposition solvent.

F. XPS Measurements. The XPS data were collected using a Leybold EA11-MCD system operating with an Al−Kα X-ray source (1486.6 eV). The analytical chamber was maintained at a steady base pressure of $<3 \times 10^{-8}$ Torr. The samples were introduced through an intermediate pumping stage by using a fast-transfer mechanical moving rod, a procedure that required a total time of approximately 5 min. All spectra were obtained using identical data collection parameters. Survey scans and high-resolution spectra were obtained by an averaging of 2 and 20 scans and using dwell times of 100 and 250 ms per point and scan, respectively. Survey spectra were obtained with a band-pass energy of 100.8 eV (spectral resolution ∼1.5 eV), whereas high-resolution spectra were obtained with a band-pass energy of 31.5 eV (spectral resolution ∼0.8 eV). All the spectra reported here were obtained using an approximate takeoff angle of 20° from the surface normal, but additional studies were carried out as a function of takeoff angle to probe the thickness and morphology of the films. High-resolution spectra were collected for the Si 2p, Zn $2p_{3/2}$, N 1s, and C 1s peaks. All the XPS peak positions were referred to the residual adventitious hydrocarbon C 1s peak at 284.6 eV. The spectra from the high-resolution scans were quantitatively analyzed by fitting them to Gaussian(20%)/Lorentian(80%) peaks after linear background subtraction using the XPS peak software.

G. AFM Measurements. The AFM measurements were made in air using a Dimension 3100 instrument and a Nanoscope IV controller housed in a class 1000 facility; the details of the procedure were adapted from studies described previously.[18] To minimize environmental noise, the experiments were run under a metal hood and the samples were locked into place by suction. The AFM tips were rotated tapping-mode etched silicon probes (RTESP) with resonant frequencies of ∼250 kHz (Veeco Probes). Height measurements were made in the tapping mode and scratches were made in the contact mode. A set point of 0.10 V was applied to all contact mode-scratching experiments because that was found suitable for removing covalently bonded molecules without affecting the Si(100) surface. The applied set-point voltage of 0.10 V was suitable for all the RTESP without prior force calibration. The AFM tip was replaced after several scratches, and the tip resonant frequency was checked after each indentation to test for damage and/or possible adherence of residue. All images were acquired with a scan rate of 1.0 Hz and were flattened with a first-order polynomial before analysis. The number of scans across the trench used to determine the mean line profiles varied from sample to sample but was typically in the 40−80 range.

H. Ellipsometry. Ellipsometric thickness measurements were carried out on a Sopra GES 5 instrument using a Xenon lamp as the light source with an intensity maximum at 450 nm. The incident angle was fixed at 75°, and the wavelength was changed from 300 to 800 nm in

(18) Anariba, F.; DuVall, S. H.; McCreery, R. L. *Anal. Chem.* **2003**, *75*, 3837−3844.

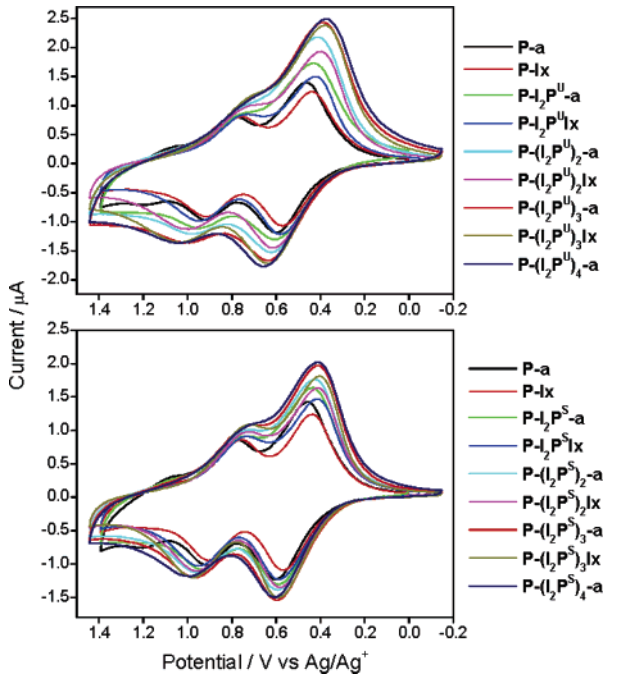

Figure 1. Fast-scan (100 V s^{-1}) voltammograms of the **P**−**a** monolayer on Si(100) and the multads formed after successive stepwise additions of BPTC and **2** (top panel) or **3** (bottom panel).

5-nm increments. The ellipsometric parameters were fitted using the Levenberg−Marquardt regression method. The film thickness was calculated using a model constructed by the Sopra Instruments group for porphyrins on Si. The model utilized initial parameters for $n(\lambda)$ and $k(\lambda)$ provided by A. R. Gallo and T. A. Sorenson (private communication).

III. Results

A key objective of our studies was to increase the charge density of our electroactive films via the formation of covalently linked porphyrin multads while simultaneously maintaining control over the film thickness. The requisite of increased charge density prompted us to first evaluate the viability of the imide-forming reaction using electrochemical methods. The results of these studies are presented first below. Although the electrochemical studies provide direct information on the charge density in the films, they do not provide insight into the structure, morphology, or thickness of the material. These physical features of the multads were evaluated in a series of studies that involved FTIR, XPS, AFM, and ellipsometric techniques. The results of these studies follow the studies of charge density.

A. Determination of Charge Density. Fast-scan (100 V s^{-1}) cyclic voltammograms of the multads formed after successive stepwise addition of 1−4 aliquots of the imide reagents (BPTC and **2** or **3**) to the **P**−**a** base layer are shown in Figure 1. The charge densities (σ) and effective surface coverages (Γ_{eff}) of the porphyrins on the planar substrate are summarized in Table 1. Inspection of the voltammetric data reveals the following salient points.

(1) The voltammetric signatures for each of the multicomponent constructs are qualitatively similar to one another and similar to that of the **P**−**a** base layer. Two redox waves, corresponding to formation of the mono- and dications of the porphyrin, are observed at ∼0.5 and ∼0.85 V, and a third, very weak wave is observed at ∼1.15 V. The voltammetric signature of **P**−**a** is somewhat distinct from that of the other Zn porphyrins, which typically exhibit only the two lower potential waves.[1−9] Our previous studies of porphyrins containing a variety of functional groups indicate that the *p*-amino functionalization of **1** (Chart 1) gives rise to atypical voltammetry.[10]

Table 1. Average Thickness (T_{ave}), Charge Density (σ), and Effective Surface Coverage (Γ_{eff}) of the Porphyrin Architectures on Si(100)

construct	T_{ave} (Å)[a] ellipsometry	AFM	XPS[b]	σ[c] (μC cm^{-2})	Γ_{eff}[d] (10^{-10} mol cm^{-2})
P−**a**	18	15	17	42	2.2
P−**Ix**	23	22		38	2.0
P−(I_2P^U)-**a**	29	30	25	59	3.1
P−(I_2P^S)-**a**	26	25		57	3.0
P−(I_2P^U)**Ix**	33	37		54	2.8
P−(I_2P^S)**Ix**	32	29		52	2.7
P−$(I_2P^U)_2$-**a**	39	43	29	81	4.2
P−$(I_2P^S)_2$-**a**	39	38		71	3.7
P−$(I_2P^U)_2$**Ix**	44			73	3.8
P−$(I_2P^S)_2$**Ix**	42			64	3.3
P−$(I_2P^U)_3$-**a**	49			95	4.9
P−$(I_2P^S)_3$-**a**	49			78	4.0
P−$(I_2P^U)_3$**Ix**	56			87	4.5
P−$(I_2P^S)_3$**Ix**	52			72	3.7
P−$(I_2P^U)_4$-**a**	67	58		98	5.1
P−$(I_2P^S)_4$-**a**	64	58		80	4.2

[a] The measured thickness of a given multad film varied by 10−20%, as determined by measurements on different samples and at different locations on a given sample (see text). [b] Measured using the ratio of the substrate signal (I_{Si}) to that of pure silicon hydride (I_{SiH}), where $T = -\lambda(E_{Si})\cos(20°)\ln(I_{Si}/I_{SH})$,[29,30] with $\lambda(E_{Si}) \approx 33$ Å. [c] Calculated from the integrated area of the $E^{0/+1}$ and $E^{+1/+2}$ anodic waves and normalized by the geometrical area of the microelectrode (10^{-4} cm^2). [d] Calculated using σ and normalized by a factor of 2 to account for the fact that each porphyrin can undergo two oxidations.

(2) As the number of components in the multad increases, the widths of the voltammetric peaks increase, and the peak-to-peak separation of the anodic and cathodic waves also increases. The changes in the peak width and peak-to-peak separation are larger for the films formed from **2** than those formed from **3**. The peak-to-peak separations do not, however, change appreciably as the scan rate is decreased from 100 V s^{-1} to 1 V s^{-1}.

(3) The charge density in the multads increases monotonically as the number of porphyrins increases (Table 1). However, the increase in charge density upon addition of the second porphyrin is only approximately 50% larger (∼60 μC cm^{-2}) than that observed for the **P**−**a** base layer (∼40 μC cm^{-2}). Interestingly, the charge densities observed for the porphyrin dyads formed by stepwise growth are very similar to those observed for layers assembled from presynthesized, diphenylethynyl-linked porphyrin dyads containing a tripodal allyl surface attachment group.[9] Upon addition of the third porphyrin, the charge density increases again by ∼20 μC cm^{-2}, but significantly less upon addition of the fourth and fifth porphyrins. This is better illustrated by plotting the charge density as a function of the nominal number of porphyrins in each oligomer, as shown in Figure 2. In this plot, the roll-off in charge density is clearly apparent in both cases, although it is much more severe in the multads formed from **3** than those formed from **2**. Finally, it should be noted that the charge density of each porphyrin-terminated multad appears to decrease slightly (by ∼10%) upon each addition of BPTC (Table 1). Thus, the charge density in each successive porphyrin-terminated multad builds off a base

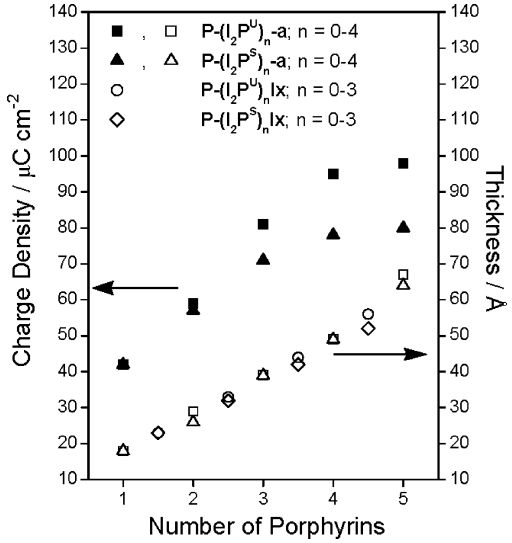

Figure 2. Plots of charge density (solid symbols) and average thickness (open symbols) versus the number of porphyrins in the multad. The thickness values are from the ellipsometric data reported in Table 1. In the thickness plot, data are also shown for the multad after each addition of BPTC; these data points fall between the porphyrin data points. In the charge-density plot, these data are not shown for clarity. Note that in both the charge density and thickness plots, certain data points overlap for the multads formed from **2** versus **3**, which somewhat compromises the appearance of the symbols.

value that is somewhat reduced from the initially obtained value. We have previously observed this phenomenon in our studies of polyimides formed from BPTC and the dianiline derivative MDA (Chart 1) atop the **P**−**a** base layer.[10]

B. Monitoring Stepwise Growth. The growth of the multads was evaluated using both FTIR and XPS methods. The FTIR studies were used to assess the formation of the imide linkage via monitoring of the vibrational signatures of the carbonyl modes of the anhydride and the imide, as we have previously described for the polyimides grown using BPTC and MDA.[10] The studies of stepwise growth were supplemented by XPS studies of selected multads, which monitored the N-atom content in the oligomers.

1. Imide Formation. The FTIR spectra of the multads formed after successive stepwise addition of 1−4 aliquots of the imide reagents (BPTC and **2** or **3**) to the **P**−**a** base layer are shown in Figure 3. The top trace in each panel is the spectrum of the **P**−**a** base layer. The key features in those spectra are the porphyrin in-plane pyrrole breathing mode at 998 cm^{-1} and the porphyrin β-hydrogen out-of-plane deformation at 797 cm^{-1}.[19] The relative intensities of these bands can be used to assess the average tilt angle of the porphyrin with respect to the surface normal, which is calculated to be ∼38° for the **P**−**a** base layer.[10] A third band of interest is that for the alkenyl hydrogen deformation at 917 cm^{-1} due to the allyl groups of porphyrin **1** (Chart 1).[20] This band is observed in the spectrum because the allyl groups of some fraction of the porphyrins in the **P**−**a** base layer do not become saturated upon binding of **1** to the surface.[10] Incomplete saturation is thought to occur because some fraction of the molecules may bind to the Si substrate via the amino group rather than the allyl tripod. Exclusive binding via the

Figure 3. FTIR spectra of the **P**−**a** monolayer on Si(100) and the multads formed after successive stepwise additions of BPTC and **2** (left panel) or **3** (right panel).

tripod, but with incomplete binding by the three allyl groups, is ruled out by studies with other triallyl-functionalized porphyrins that lack the *p*-amino group, for which complete saturation of the allyl groups is observed upon binding to Si.[8,9] The presence of "inverted" molecules in the **P**−**a** base layer has clear implications for the growth of the oligomers (vide infra).

Upon the addition of BPTC (second traces in Figure 3), the vibrational signatures of the porphyrin remain, but new features appear due to the appended BPTC. The key bands are observed at 1852, 1778, and 1724 cm^{-1}, all of which are due to C═O stretches of the anhydride and/or imide:[21,22] the 1852-cm^{-1} band is due to the symmetric C═O stretch of the anhydride, the 1778-cm^{-1} band is due primarily to the asymmetric C═O stretch of the anhydride (which overlaps the weaker symmetric C═O stretch of the imide), and the 1724-cm^{-1} band is due to the asymmetric C═O stretch of the imide. Interestingly, the 917-cm^{-1} band of the allyl group disappears upon reaction with BPTC. We have no explanation for this observation, because the reagents used for imide formation should not react with the alkene. Upon the addition of **2** or **3** (third traces in Figure 3), the 1852-cm^{-1} band of the anhydride disappears, the intensity of the 1778-cm^{-1} band is greatly attenuated, and the intensity

(19) (a) Li, X. Y.; Czernuszewicz, R. S.; Kincaid, J. R.; Su, Y. O.; Spiro, T. G. *J. Phys. Chem.* **1990**, *94*, 31−47. (b) Li, X. Y.; Czernuszewicz, R. S.; Kincaid, J. R.; Spiro, T. G. *J. Am. Chem. Soc.* **1989**, *111*, 7012−7023.

(20) Silverstein, R. M.; Bassler, G. C. *Spectrophotometric Identification of Organic Compounds*; Wiley: New York, 1967.

(21) Hase, Y.; Davanzo, C. U.; Kawai, K.; Sala, O. *J. Mol. Struct.* **1976**, *30*, 37−44.

(22) (a) Debe, M. K. *J. Vac. Sci. Technol.* **1982**, *21*, 74−79. (b) Tsai, W. H.; Boerio, F. J.; Jackson, K. M. *Langmuir* **1992**, *8*, 1443−1450.

of the 1724-cm^{-1} band of the imide increases, consistent with the loss of all available anhydride and quantitative formation of an additional imide linkage (heating the **P**−**Ix** layer in the absence of the **2** or **3** does not alter the anhydride bands). The carbonyl-band intensity pattern exhibits a similar alteration upon addition of the next aliquots of BPTC and **2** or **3** (fourth and fifth traces in Figure 3), and this pattern is repeated for all subsequent additions of BPTC and **2** or **3**. It should be noted that the reaction of an amine with an anhydride is believed to proceed via the acid−amide (not shown) to the imide.[23] We observe no spectroscopic features characteristic of a free carboxylic acid.

There are several noteworthy features observed in the FTIR spectra of the multads, including the following:

(1) Upon addition of each aliquot of **2** or **3**, the vibrational bands due to the terminal anhydride of the previously formed multad completely disappear, suggesting that all of the available anhydride reacts. This observation does not, however, imply that BPTC quantitatively reacted with all of the amino-terminated porphyrins in the previous multad. Plausibly, certain porphyrins might be inaccessible to the reagent at a particular step. Unfortunately, the coupling to BPTC cannot be easily quantified using the vibrational spectra, because bands key to monitoring this reaction such as the NH_2 stretching or bending modes are not clearly observed.

(2) The absolute intensity of the vibrational bands of the porphyrins increases as the number of porphyrins in the multads increases. However, the total intensity increase from the **P**−**a** base layer to the multad that nominally contains five porphyrins is only approximately 1.5. This value is less than the factor of 2−2.5 indicated by the electrochemical measurements of charge density (Table 1).

(3) The intensity of the C═O bands of the imide increase monotonically as the number of imide linkages increases. Unlike the behavior of the porphyrin bands, the increase in the intensity of the imide C═O bands is qualitatively commensurate with the number of linkages formed.

Finally, we note that the interpretation of the changes in intensity (both absolute and relative) of the vibrational bands of the surface-bound molecules is complicated by the fact that these intensities are also affected by the orientation of the transition dipole moments with respect to the surface.[24] These orientation effects may be responsible for the less than expected increase in the intensity of the porphyrin bands, both overall and with respect to the imide bands. In principle, a complete analysis of the intensities of the vibrational bands could provide detailed information concerning the orientation of the molecules in the multads. However, such an analysis is not feasible because the torsional flexibility of the phenyl rings of BPTC as well as those of the porphyrin are expected to result in a highly nonlinear oligomer, which may also exhibit multiple torsional conformations.

2. N-Atom Content. A representative XPS survey of the **P**−**a** monolayer is shown in Figure 4. The spectrum is typical of that of other porphyrin monolayers on Si(100) and exhibits multiple peaks consistent with the molecular composition of the porphyrins. In particular, in addition to signals from the bulk Si, the spectra show discrete signals for Zn and N. Moreover, the high-resolution Zn $2p_{3/2}$ and N 1s spectra (Figure 4, insets) show peaks at binding energies of 1021.6 ± 0.1 and 398.3 ± 0.1 eV, respectively, in qualitative agreement with values previously reported for Zn porphyrins.[11,25−27] Closer inspection of the high-resolution XPS in the N 1s region reveals a second peak (designated N(2), to differentiate it from the main feature from the porphyrin, denoted N(1)) at 400.5 eV ± 0.1, which is not observed for Zn porphyrins without the *p*-amino group. This is illustrated in Figure 5 (upper panels), which compares the high-resolution N 1s regions of the **P**−**a** monolayer (top right panel) with that of a monolayer of an analogous Zn porphyrin lacking the *p*-amino group, designated **P** (top left panel). The

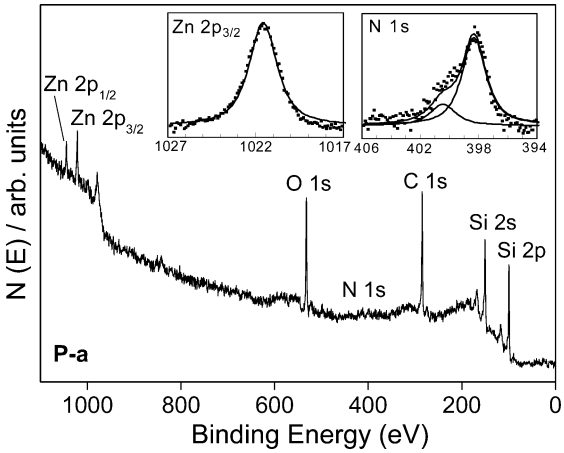

Figure 4. Survey XPS for the **P**−**a** monolayer on Si(100). (Insets) High-resolution scans of the Zn $2p_{3/2}$ and N 1s spectral regions: raw data (dots) and fits (solid).

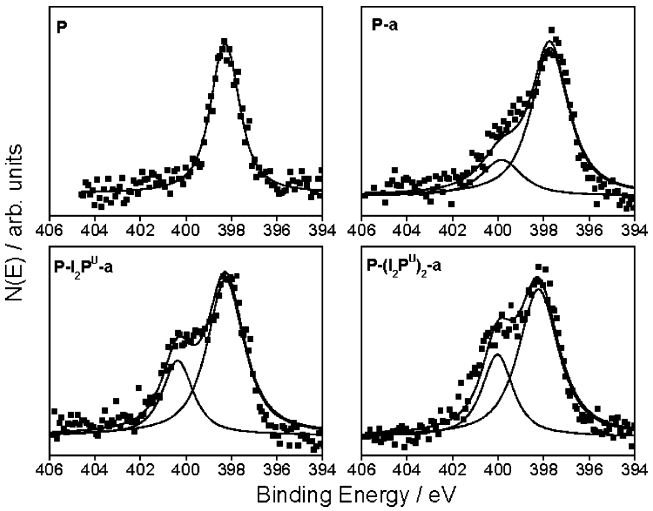

Figure 5. High-resolution XPS for the **P**−**a** monolayer (top right) and the **P**−$\mathbf{I_2P^U}$−**a** and **P**−$\mathbf{(I_2P^U)_2}$−**a** multads (bottom) in the N 1s spectral region. For comparison, the XPS of a monolayer of a porphyrin that lacks the *p*-amino group (**P**) is also shown (top left).

(23) *Polyimides: Fundamentals and Applications*; Ghosh, M. K., Mittal, K. L., Eds.; Marcel Dekker: New York, 1996.
(24) (a) Greenler, R. G. *J. Chem. Phys.* **1966**, *44*, 310−315. (b) Allara, D. L.; Nuzzo, R. G. *Langmuir* **1985**, *1*, 52−66. (c) Zaera, F. *Int. Rev. Phys. Chem.* **2002**, *21*, 433−471.
(25) Polzonetti, G.: Ferri, A.; Russo, M. V.; Iucci, G.: Licoccia, S.; Paolesse, R. *J. Vac. Sci. Technol., A* **1999**, *17*, 832−839.
(26) Zhang, Z.; Hu, R.; Liu, Z. *Langmuir* **2000**, *16*, 1158−1162.
(27) (a) Yasseri, A. A.; Syomin, D.; Malinovskii, V.; Loewe, R. S.; Lindsey, J. S.; Zaera, F.; Bocian, D. F. *J. Am. Chem. Soc.* **2004**, *126*, 11944−11953. (b) Yasseri, A. A.; Sykomin, D.; Loewe, R. S.; Lindsey, J. S.; Zaera, F.; Bocian, D. F. *J. Am. Chem. Soc.* **2004**, *126*, 15603−15612. (c) Wei, L.; Tiznado, H.; Liu, G.; Padmaja, K.; Lindsey, J. S.; Zaera, F.; Bocian, D. F. *J. Phys. Chem. B* **2005**, *109*, 23963−23971.

Table 2. XPS Binding Energies and Atomic Ratios for the **P**−**a**, **P**−$\mathbf{I_2P^U}$−**a**, and **P**−$\mathbf{(I_2P^U)_2}$−**a** Architectures on Si(100)

	binding energy (eV)[a]				atomic ratio[b]		
construct	Si 2p	Zn $2p_{3/2}$	N 1s (1)	N 1s (2)	Zn:N(1)	Zn:N(2)	N(1):N(2)
P−**a**	99.2	1021.6	398.3	400.5	1:3.7 ± 0.2	1:0.98 ± 0.04	3.8 ± 0.3:1
P−$\mathbf{I_2P^U}$−**a**	99.1	1021.4	398.4	400.5	1:3.6 ± 0.2	2:2.8 ± 0.1	7.5 ± 0.6:3
P−$\mathbf{(I_2P^U)_2}$−**a**	99.1	1021.4	398.2	400.1	1:3.8 ± 0.2	3:4.9 ± 0.2	11.6 ± 0.9:5

[a] All binding energies are accurate within ±0.1 eV. [b] Calculated using the reported atomic sensitivity factors for Zn $2p_{3/2}$ and N 1s, and corrected for the kinetic dependence of the spectrometer detection efficiency and effects due to depth of the atoms from the surface of the film.

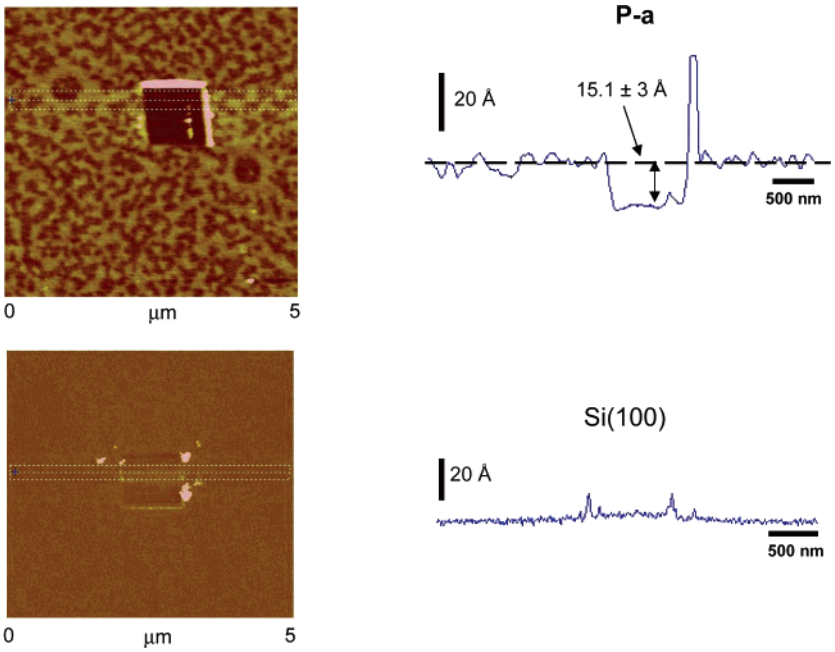

Figure 6. AFM images and mean line profiles for the Si(100) surface before attachment of porphyrin **1** and after formation of the **P**−**a** monolayer. (Lower left) Tapping mode image of the hydrogen passivated Si(100) surface displaying a 1 × 1 μm^2 scratch made in contact mode. (Lower right) Mean line profile through the indentation made on the surface shown in the lower left image. (Upper left) Tapping mode AFM image of the **P**−**a** monolayer showing a 1 × 1 μm^2 trench in the monolayer formed in contact mode. (Upper right) Mean line profile across the trench in the upper left image.

values of the Zn:N(1):N(2) atomic ratios, obtained by scaling the peak intensities using known atomic cross-section sensitivity factors and correcting for the expected photoelectron attenuation due to the film thickness,[28] are in an approximate 1:4:1 stoichiometry. This is consistent with the N(2) XPS peak being assigned to the N atom of the *p*-amino group. The peaks due to the porphyrin and amino N atoms are highly overlapped, so it is not possible to distinguish between free versus surface-bound N atoms in the *p*-amino group. Therefore, the XPS data cannot be used to settle the issue of the potential binding of some fraction of the molecules in the base layer to the Si substrate via the amino group rather than the allyl tripod.

XP spectra were also obtained for the multads containing two and three porphyrins (only multads formed upon addition of **2** were studied here). The survey spectra of the multads are similar to those of the **P**−**a** base layer, and are not shown, but the N 1s high-resolution XP spectra of the multads composed of two- and three-porphyrins are included in the bottom panels of Figure 4. Also, the binding energies and atomic ratios for all three constructs are summarized in Table 2. The key observation in the spectra of the multads is that the intensity of the N(2) peak increases relative to the porphyrin N(1) peak. Indeed, the N(1):N(2) atomic ratios for the **P**−**a** base layer and the two- and three-porphyrin multads are 3.8 ± 0.3:1, 7.5 ± 0.6:3, and 11.6 ± 0.9:5, respectively, in qualitative agreement with the expected relative stoichiometry of the *p*-amino/imido N-atom versus porphyrin N-atom content of the oligomers (Chart 2). It should be noted, however, that the errors in the relative intensities are relatively large, owing to the severe overlap of the N(1) and N(2) peaks combined with the S/N ratio of the data. These factors mask any disparities in the N(1):N(2) atomic ratios that would arise because (1) certain porphyrins in the **P**−**a** base layer are likely "inverted" and cannot react to form imide linkages and/or (2) certain properly oriented porphyrins in the **P**−**a** base layer (and in the imide-linked multads) might not react with BPTC.

C. Determination of Multad Film Morphology and Thickness. The morphologies and thicknesses of the **P**−**a** base layer and selected porphyrin multad films were interrogated by using AFM. In addition, the thicknesses of all the films were examined via ellipsometry, and those of a limited number of films were also estimated from the XPS data. The AFM images and mean line profiles for selected multad films are shown in Figures 6 and 7. The average thickness (T_{ave}) obtained for the films via the different methods is summarized in Table 1 along with the charge densities (σ) and effective surface coverages (Γ_{eff}) of the porphyrins in the films. The T_{ave} values obtained for the films via ellipsometry are also plotted in Figure 2 along with the σ values.

(28) Wagner, C. D.; Riggs, W. M.; Davis, L. E.; Moulder, J. F.; Muilenberg, G. E.; *Handbook of X-ray Photoelectron Spectroscopy*; Perkin-Elmer Corp.: Eden Prairie, MN, 1978.

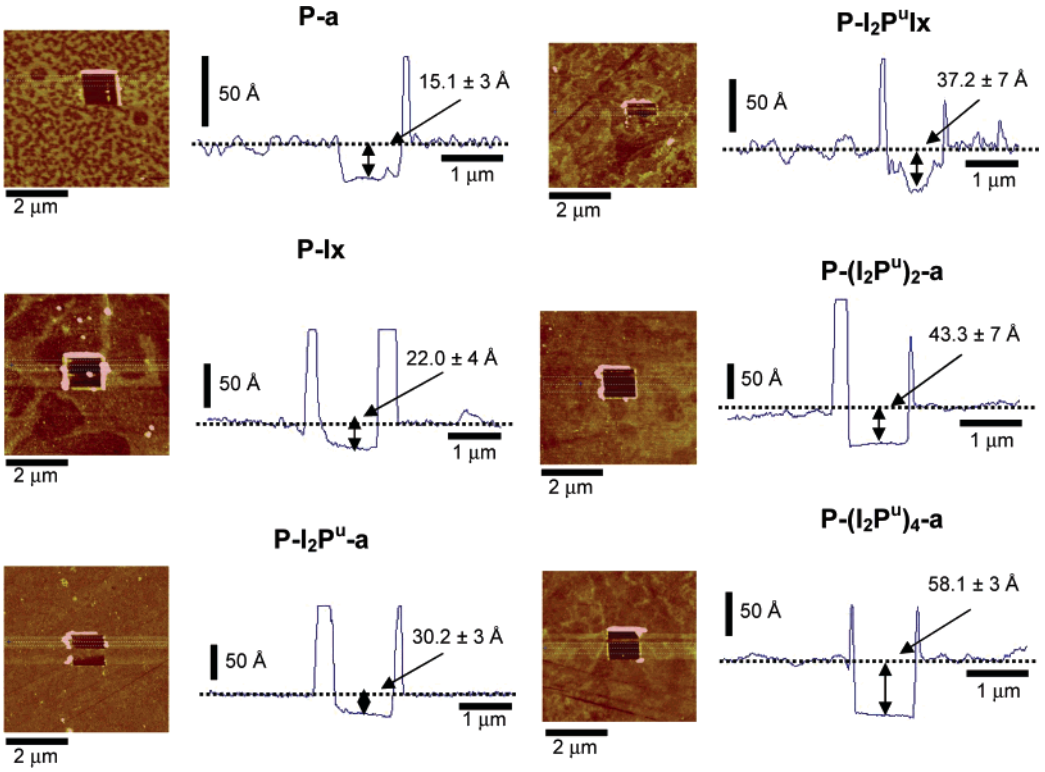

Figure 7. AFM images and mean line profiles for the **P**−**a** monolayer and for selected multad films formed after addition of BPTC and **2**.

The AFM images of the **P**−**a** base layer are compared with those of a bare Si−H surface in the left panels of Figure 6, whereas the mean line profiles obtained by scratching the two different surfaces are shown in the corresponding right panels. Inspection of these data shows that the **P**−**a** base layer has a much rougher appearance (thickness variation ≈ 20%), than the Si−H surface which is also reflected in the much larger background fluctuation of the mean line profile for the monolayer. The roughened appearance of the **P**−**a** monolayer can be contrasted with that observed for an analogous porphyrin that lacks the *p*-amino group (not shown); the appearance of this latter porphyrin monolayer is qualitatively more similar to that of the Si−H surface than to that of the **P**−**a** layer. The AFM images and mean line profiles for selected porphyrin multad films are shown in Figure 7. These data reveal that the multad films also exhibit roughness but that the thicker films appear somewhat smoother (thickness variation ≈ 10%) than the thinner films. Angle-resolved XPS data on these films corroborates qualitatively the general morphology trends seen by AFM.

Comparison of the average thickness (T_{ave}) values for the various multads obtained via ellipsometry, AFM, and XPS techniques reveals that all three methods yield similar film thicknesses to within experimental error (Table 1). The possible exception is the value for the thickness of the three-porphyrin multad measured via XPS. The thickness of the **P**−**a** base layer is in the 15−18 Å range, which is qualitatively consistent with that expected on the basis of the approximate end-to-end length of porphyrin **1** (∼25 Å from the distal amino group to the Si surface, assuming an all-trans conformation of the propyl tethers) taking into account that the molecule is tilted on the surface (38° with respect to the surface normal, according to the infrared data).[10] The T_{ave} value increases monotonically upon each successive addition of BPTC and **2** or **3**, but the increase in thickness is ∼5 Å per added unit of either BPTC or **2** (or **3**), significantly less than the end-to-end length of either the BPTC (∼10 Å between the bridging oxygen atoms of the dianhydride, assuming a trans conformation) or the porphyrins (∼25 Å). Fits of T_{ave} versus the number of molecules nominally in each oligomer are quite linear ($R > 0.99$), which is surprising given that the end-to-end length of the BPTC molecules is less than half that of the porphyrins. Also noteworthy is the fact that the T_{ave} value continues to increase after the σ value rolls off.

IV. Discussion

The studies reported herein demonstrate that ultrathin porphyrin multad films of relatively well-controlled thickness can be grown in a stepwise fashion using the imide-forming reaction. The ability to assemble such architectures provides a convenient means of increasing the charge density in redox-active media in a relatively well-controlled fashion. Given that the ultimate control over charge density is determined by the physical characteristics of the multads, our studies have focused on this aspect of the problem. Below, we discuss the fundamental properties of the multiporphyrin architectures constructed using our methodology and how the stepwise addition of porphyrin components provides for increased charge density.

Our previous studies of **P**−**a** monolayers have shown that a certain fraction of the molecules are likely bound to the Si surface via the amino group rather than the triallyl tripod.[10] The exact percentage of "inverted" molecules is uncertain, but the presence of these structures in the base layer precludes some imide formation in the initial reaction with BPTC. This is a major factor in the reduction in efficiency when building porphyrin oligomers using our step-by-step derivatization methodology. Indeed, the presence of unreactive species in the

base layer is qualitatively consistent with the charge densities achieved upon addition of the second porphyrin, which are only about 50% larger than those obtained for the **P**−**a** base layer. Plausibly, this observation could imply an equal distribution of correctly versus incorrectly oriented molecules in the **P**−**a** base layer. However, it is also possible that the reaction with BPTC is less than quantitative, a possibility that is not clearly delineated by the spectroscopic data. In this regard, we have attempted to increase the fraction of correctly oriented molecules in the base layer by using a version of porphyrin **1** wherein the amino group is flanked by methyl groups (which should sterically impede attachment via the amino group). However, electrochemical studies using this molecule as a base layer (unpublished results) indicate that the increase in charge density achieved via addition of the second porphyrin is quite similar to that achieved when porphyrin **1** forms the base layer.[31] Based on those initial observations, we tend to favor the view that the reaction of the correctly oriented molecules in the **P**−**a** base layer with BPTC may not be quantitative, perhaps because of steric constraints imposed by the relatively well-packed porphyrins in the base layer. Regardless of the degree of completeness of the initial reaction of BPTC with the **P**−**a** base layer, the reaction of the **P**−**Ix** construct with either **2** or **3** appears to be quantitative, as is evidenced by the complete disappearance of vibrational features due to the anhydride. Likewise, at all steps in the formation of the multads, the reaction of the anhydride-terminated multad with the incoming amino-porphyrin appears to be quantitative. What remains uncertain is whether the reaction of the amino-terminated multads with incoming BPTC molecules is quantitative.

The morphology and thickness of the multad films provides additional insight into their probable composition. In particular, all of the films appear somewhat rough, with height variations of 10−20%. This characteristic of the multad films suggests some degree of heterogeneity in the composition of the individual oligomers. This view is supported by the observation that the increases in thickness of the film with each successive addition of BPTC and **2** or **3** are considerably less than those expected for uniform growth of each of the individual oligomers. Thus, it appears that the thickness measurements are sampling an ensemble average of a distribution of oligomers with different numbers of components. We also note that the smaller-than-expected increases in thickness may be due, at least in part, to the torsional flexibility of the porphyrin and BPTC components about the phenyl groups, which will lead to nonlinear structures. Thus, the oligomers are likely to exhibit some degree of both structural and conformational heterogeneity. These characteristics of the oligomers may in fact be interdependent. In particular, the conformational flexibility may result in entanglement of adjacent oligomers, which in turn could inhibit reaction when adding the next BPTC. In a highly nonlinear and entangled collection of oligomers, it is also possible that the growth of a given pair of oligomers might be terminated by coupling of their ends via the incoming difunctionalized reagent.

Another noteworthy aspect of the characteristics of the multads is that the charge density appears to roll off after the addition of the third or fourth porphyrin to the base layer, despite the fact that the average thickness of the films continues to increase. This feature might signal that the overall efficiency of the coupling reaction to BPTC diminishes as the film thickness increases. If so, the conformation of surface-distal portions of the longer oligomers must be different from that of the surface-proximal portion (to maintain a near constant increase in average thickness). On the other hand, the charge-density roll-off might also signal that certain porphyrins in the multads are electrochemically inactive, which might arise if solvent and/or counterions cannot penetrate the films. Interestingly, the charge density roll-off for multads formed from **3** is more severe than for those formed from **2**. The methyl groups flanking the amino groups of **3** are expected to result in less torsional flexibility of the phenyl groups of the porphyrin, which might inhibit dynamic fluctuations and allow for reduced penetration of the solvent and/or electrolyte into film. Regardless of the origin of the charge-density roll-off, the inability to further increase this property is a limitation of the multads formed from these particular building blocks for charge-storage applications. Nonetheless, the high charge density already achieved with multads comprised of 3−5 porphyrins (up to ∼90 μC cm^{-2}) greatly exceeds that of Si/SiO_2-based capacitors (1−2 μC cm^{-2}).

Acknowledgment. This work was supported by the DARPA/DMEA (Award Nos. H94003-04-2-0404 and H94003-05-2-0504) and by ZettaCore, Inc. We thank Drs. A. R. Gallo and T. A. Sorenson for providing the ellipsometric parameters for the porphyrins on Si.

JA060906Q

(29) Paynter, R. W. *Surf. Interface Anal.* **1981**, *3*, 186−187.
(30) Boekl, M. S.; Bramblett, A. L.; Hauch, K. D.; Sasaki, T.; Ratner, B. D.; Rogers, J. W., Jr. *Langmuir* **2000**, *16*, 5644−5653.
(31) Plausibly the similar charge densities observed upon addition of the second porphyrin to the base layer formed from **1** and the version of **1** containing the methyl-flanked amino group arise from compensating effects wherein more of the latter porphyrin is correctly oriented, but formation of the first imide (via reaction with BPTC) is impeded owing to steric constraints from the methyl groups flanking the amino group on the base porphyrin. An argument against this interpretation is that imide formation between the **P**−**Ix** layer and either **2** or **3** appears to be quantitative and yields dyad films of similar charge density (Table 1).